J. Fluid Mech. (1996), *vol.* 320, *pp.* 369–394

Stability of stratified flow of large depth over finite-amplitude topography

By DILIP PRASAD, JAIME RAMIREZ AND T. R. AKYLAS

Department of Mechanical Engineering, Massachusetts Institute of Technology
Cambridge, MA 02139, USA

(Received 10 July 1995 and in revised form 4 April 1996)

The flow of a Boussinesq density-stratified fluid of large depth past the algebraic mountain ('Witch of Agnesi') is studied in the hydrostatic limit using the asymptotic theory of Kantzios & Akylas (1993). The upstream conditions are those of constant velocity and Brunt–Väisälä frequency. On the further assumptions that the flow is steady and there is no permanent alteration of the upstream flow conditions (no upstream influence), Long's model (Long 1953) predicts a critical amplitude of the mountain ($\epsilon = 0.85$) above which local density inversions occur, leading to convective overturning. Linear stability analysis demonstrates that Long's steady flow is in fact unstable to infinitesimal modulations at topography amplitudes below this critical value, $0.65 \lesssim \epsilon < 0.85$. This instability grows at the expense of the mean flow and may be attributed to a discrete spectrum of modes that become trapped over the mountain in the streamwise direction. The transient problem is also solved numerically, mimicking impulsive startup conditions. In the absence of instability, Long's steady flow is reached. For topography amplitudes in the unstable range $0.65 \lesssim \epsilon < 0.85$, however, the flow fluctuates about Long's steady state over a long timescale; there is no significant upstream influence and no evidence of transient wave breaking is found for $\epsilon \leqslant 0.75$.

1. Introduction

The present investigation is concerned with the flow of density-stratified fluid over an obstacle of finite amplitude. This problem was first studied systematically by Long (1953), who devised an analytical model that accounts, under specific flow conditions, for finite-amplitude effects. Long's model hinges on the fact that the equations governing inviscid, steady, two-dimensional flow reduce to a linear form for certain background velocity and density profiles under the hypothesis that the topography does not alter these profiles far upstream – the so-called assumption of no 'upstream influence'. In particular, for a weakly stratified (Boussinesq) fluid, Long's model applies when the upstream velocity and Brunt–Väisälä frequency are independent of height. According to this model, given the topography shape and for fixed values of the other flow parameters, there is a critical amplitude of the obstacle above which the predicted steady flow features locally reversed density gradients ('breaking' streamlines) that would result in static instability (see, for example, Miles 1969).

In more recent work, Kantzios & Akylas (1993, hereinafter referred to as KA) proposed an asymptotic theory that describes the long-time dynamics of vertically

unbounded stratified flow over extended finite-amplitude topography; this flow configuration is most relevant to atmospheric applications (Baines 1987) and is also the subject of the present study. The approach of KA generalizes Long's model by allowing for slightly unsteady disturbances with the proviso that wave breaking is not present. Within this framework, it is then possible to examine the realizability of Long's steady states for subcritical topography amplitudes (below that required to cause overturning).

The problem of stratified flow of large depth over topography has also been studied extensively through direct numerical simulations. These studies solve the full Euler equations of motion in a finite computational domain, imposing the radiation condition at the upper boundary via a 'sponge layer', and are not limited to flow conditions that preclude wave breaking.

Specifically, Clark & Peltier (1977), Pierrehumbert & Wyman (1985) and Laprise & Peltier (1989*a*,*b*), among others, concentrate on two-dimensional Boussinesq flow with constant velocity and Brunt–Väisälä frequency far upstream past the algebraic mountain ('Witch of Agnesi'). They all appear to agree that the steady state furnished by Long's model is reached as long as the amplitude of the topography is subcritical. In another numerical study of the same problem, however, Pierrehumbert & Bacmeister (1987) find that instability may occur at a slightly subcritical (about 5%) topography amplitude owing to convective overturning induced by transient effects. Moreover, the simulations of Laprise & Peltier (1989*a*,*b*) reveal that the dominant instability mechanism even for slightly supercritical topography is of a shear-flow type, owing to the steepening of streamlines of the background flow over the topography.

Pierrehumbert & Bacmeister (1987) also discussed the assumption of no upstream influence in the context of related experimental observations by Baines & Hoinka (1985). The experiments were conducted in a novel apparatus to simulate an infinite medium, and revealed upstream motions at significantly subcritical amplitudes, suggesting that Long's model ceases to be valid at relatively low obstacle steepness. In their numerical simulations, however, Pierrehumbert & Bacmeister (1987) did not observe any permanent alterations in the upstream flow field, and cautioned that slowly varying transient disturbances could be mistaken for true upsteam influence.

In the present paper, we shall discuss the dynamics of nonlinear stratified flow over topography on the basis of the asymptotic theory of KA. We concentrate on the simplest case of uniformly stratified hydrostatic flow of large depth over the algebraic mountain which, as already mentioned, has also been explored in previous numerical work. There is, in fact, numerical evidence that this flow quickly evolves into a quasi-steady Long state as long as the topography amplitude is not highly supercritical (Pierrehumbert & Bacmeister 1987); the flow dynamics is then controlled by slowly varying disturbances, making the asymptotic theory most relevant.

The ensuing analysis centres on two main issues: the stability of Long's steady state for subcritical topography amplitudes and the long-time behaviour of the flow when this state is unstable. Based on the evolution equations derived in KA, a linear stability analysis of Long's state to infinitesimal modulations is carried out first. Instability sets in at a topography amplitude well below (by about 25%) the critical value for overturning, owing to a shear-flow mechanism brought about by the steepening of streamlines of the steady flow over the topography. The transient flow development in the unstable régime is then studied by integrating the evolution equations numerically, starting from rest. The effect of instability turns out to be rather subdued: the flow oscillates slowly about the corresponding Long steady state and no transient breaking is found for subcritical topography amplitudes within 10%

of the critical value. These findings are discussed in connection with previous related work at the end of the paper.

2. Preliminaries

Consider the flow of an inviscid, incompressible, vertically unbounded stratified fluid past a two-dimensional obstacle having peak height h and horizontal dimension L. Far upstream of the topography, the fluid is assumed to have uniform stratification (constant Brunt–Väisälä frequency N_0) and constant velocity U_0. The acceleration due to gravity is denoted by g. These flow quantities may be combined to yield three non-dimensional parameters:

$$\mu = \frac{U_0}{N_0 L}, \qquad \beta = \frac{N_0 U_0}{g}, \qquad \epsilon = \frac{N_0 h}{U_0}.$$

Here μ measures dispersive effects, β is the Boussinesq parameter which is a measure of stratification, and ϵ controls nonlinear effects.

Scaling the horizontal (streamwise) coordinate x with L, the vertical coordinate y with U_0/N_0 and time t with L/U_0, the governing equations of incompressibility, mass conservation and momentum balance may be cast in non-dimensional form as

$$\nabla \cdot \boldsymbol{u} = 0, \tag{2.1}$$

$$\rho_t + \boldsymbol{u} \cdot \nabla \rho = 0, \tag{2.2}$$

$$\beta \rho (\boldsymbol{u}_t + \boldsymbol{u} \cdot \nabla \boldsymbol{u}) = -\left(p_x,\ \mu^{-2}(\rho + p_y)\right), \tag{2.3}$$

where $\boldsymbol{u} = (u, v)$ is the velocity field, and p and ρ are the pressure and density respectively. The boundary condition of zero normal velocity on the topography $y = \epsilon f(x,t)$ is

$$v = \epsilon(u f_x + f_t) \qquad (y = \epsilon f). \tag{2.4}$$

The asymptotic theory of KA describes the dynamics of finite-amplitude, long-wave disturbances in a Boussinesq fluid. In terms of the non-dimensional parameters introduced above, this régime corresponds to $\mu \ll 1$, $\beta \to 0$, $\epsilon = O(1)$. Here we shall only outline the salient features of the theory; details may be found in the original paper.

The theory is motivated by the observation that, in the hydrostatic limit ($\mu \to 0$), Long's steady state consists of a long-wave mode with vertical wavenumber equal to unity. The corresponding group velocity vanishes in the reference frame of the obstacle; energy is therefore trapped near the topography and the transient response is expected to develop slowly. This resonance suggests that the long-time response takes the form of a slowly varying Long state, in line with the results of numerical simulations noted earlier (Pierrehumbert & Bacmeister 1987).

Accordingly, the streamfunction $\psi(x, y, T)$ is posed as

$$\psi \sim \psi^{(0)} = y + (A\, \mathrm{e}^{\mathrm{i}y} + \text{c.c.}). \tag{2.5}$$

Here $A(x, Y, T) = a + \mathrm{i}b$ denotes the complex envelope of the resonant long-wave mode; it accounts for the evolution of the disturbance in terms of the 'slow' time $T = \mu^2 t$ and the 'stretched' vertical coordinate $Y = \mu^2 y$. As explained in KA, one may obtain evolution equations for the real amplitudes a and b following a perturbation procedure, and thereby describe the long-time dynamics of the flow through (2.5).

Briefly, deriving these amplitude equations makes use of the fact that, if one neglects

transient effects altogether, the density ρ and the quantity

$$S = \rho\psi_{yy} + \rho_\psi\left(\frac{y}{\beta} + \tfrac{1}{2}\psi_y^2\right) \tag{2.6}$$

remain constant along streamlines. This suggests replacing the coordinate y by ψ:

$$(x, y, T) \to (x, \psi, T)$$

on the condition that no flow reversal (wave breaking) is present in the flow field. The mass-conservation equation (2.2) then takes the form

$$\psi_y \rho_x|_\psi = -\mu^2 \rho_T, \tag{2.7}$$

and the momentum equations (2.3) can be manipulated to

$$\psi_y S_x|_\psi = \mu^2\{\rho(\psi_x\psi_{xy} - \psi_y\psi_{xx})\}_x - \mu^2(\rho\psi_{yT})_y + \left\{\rho_x|_\psi\left(\frac{y}{\beta} + \tfrac{1}{2}\psi_y^2\right)\right\}_y, \tag{2.8}$$

where $|_\psi$ indicates that ψ is held fixed.

Using the upstream conditions of uniform stratification and constant velocity and invoking the Boussinesq approximation $\beta \to 0$, (2.7) and (2.8) may be integrated to yield

$$\rho = \rho_0(\psi) - \mu^2\rho_{0\psi}\int_{-\infty}^{x}\left.\frac{\psi_T}{\psi_y}\right|_\psi \mathrm{d}x', \tag{2.9}$$

$$S = -\rho_0(\psi)\psi - \mu^2\rho_0(\psi)\psi_{xx} - \mu^2\int_{-\infty}^{x}\left.\frac{R}{\psi_y}\right|_\psi \mathrm{d}x' \tag{2.10}$$

with $$R = \rho_0(\psi)\{\psi_{yyT} - (y\psi_T/\psi_y)_y\},$$

$\rho_0(y)$ being the (known) density upstream.

Making use of (2.6) and (2.9), (2.10) may be rearranged as

$$\psi_{yy} + (\psi - y) = \mu^2(H - \psi_{xx}), \tag{2.11}$$

where

$$H = \frac{\partial}{\partial\psi}\int_{-\infty}^{x}\left\{y\frac{\psi_T}{\psi_y} - \psi_{yT}\right\}\Big|_\psi \mathrm{d}x' - y\frac{\partial}{\partial\psi}\int_{-\infty}^{x}\left.\frac{\psi_T}{\psi_y}\right|_\psi \mathrm{d}x'.$$

As expected, if transient effects (the term involving H above) are neglected, (2.11) becomes linear and Long's steady-flow model is recovered.

To describe the flow evolution, we work with (2.11) and follow a multiple-scale perturbation procedure: the streamfunction ψ is expanded as

$$\psi = \psi^{(0)} + \mu^2\psi^{(1)} + \cdots,$$

where $\psi^{(0)}$ is the slowly modulated Long's solution (2.5) proposed earlier on physical grounds. In terms of the envelope $A = a + \mathrm{i}b$, the boundary condition (2.4) on the topography is also cast in the form (to leading order in μ)

$$a\cos\epsilon f - b\sin\epsilon f = -\tfrac{1}{2}\epsilon f \qquad (Y = 0). \tag{2.12}$$

At the next order in μ, the following equation is obtained:

$$\psi^{(1)}_{yy} + \psi^{(1)} = H^{(0)} - \psi^{(0)}_{xx} - 2\psi^{(0)}_{yY}, \tag{2.13}$$

where the superscript $^{(0)}$ indicates that the quantity is to be evaluated using the known expression (2.5) for $\psi^{(0)}$. The desired evolution equations for the amplitudes $a(x, Y, T)$

and $b(x, Y, T)$ are then obtained by imposing secularity conditions on the right-hand side of (2.13):

$$\frac{1}{4\pi}\int_0^{2\pi} H^{(0)} \cos y \, \mathrm{d}y - \tfrac{1}{2}a_{xx} + b_Y = 0, \tag{2.14a}$$

$$\frac{1}{4\pi}\int_0^{2\pi} H^{(0)} \sin y \, \mathrm{d}y + \tfrac{1}{2}b_{xx} + a_Y = 0. \tag{2.14b}$$

As already indicated, we shall focus on purely hydrostatic flow, in which case the dispersive terms involving a_{xx}, b_{xx} in (2.14) are dropped. Furthermore, based on the assumption made earlier that precludes wave breaking, the flow field described by (2.5) is such that y is defined uniquely as a function of $\psi^{(0)}$, $y = y(\psi^{(0)}; a, b)$, and one may replace the y-integrations with $\psi^{(0)}$-integrations in (2.14). After this change of integration variable is implemented and one differentiation with respect to x, (2.14) reduce to

$$K_{11}^c a_T + K_{12}^c b_T + b_{xY} + \int_{-\infty}^{x} \mathrm{d}x' \left(K_{11x} a'_T + K_{12x} b'_T\right) = 0, \tag{2.15a}$$

$$K_{21}^c a_T + K_{22}^c b_T - a_{xY} + \int_{-\infty}^{x} \mathrm{d}x' \left(K_{21x} a'_T + K_{22x} b'_T\right) = 0. \tag{2.15b}$$

Here the kernels $K_{11}, \ldots, K_{22}$ are defined by

$$K_{11}(x, x') = \frac{1}{8\pi}\int_0^{2\pi} \mathrm{d}\psi^{(0)} y_a \left(y'_a + (y' y'_a)_{\psi^{(0)}} - y y'_{a\psi^{(0)}}\right), \tag{2.16a}$$

$$K_{12}(x, x') = \frac{1}{8\pi}\int_0^{2\pi} \mathrm{d}\psi^{(0)} y_a \left(y'_b + (y' y'_b)_{\psi^{(0)}} - y y'_{b\psi^{(0)}}\right), \tag{2.16b}$$

$$K_{21}(x, x') = \frac{1}{8\pi}\int_0^{2\pi} \mathrm{d}\psi^{(0)} y_b \left(y'_a + (y' y'_a)_{\psi^{(0)}} - y y'_{a\psi^{(0)}}\right), \tag{2.16c}$$

$$K_{22}(x, x') = \frac{1}{8\pi}\int_0^{2\pi} \mathrm{d}\psi^{(0)} y_b \left(y'_b + (y' y'_b)_{\psi^{(0)}} - y y'_{b\psi^{(0)}}\right), \tag{2.16d}$$

with the notation that primed variables are functions of x', and $K_{11}^c \equiv K_{11}(x, x), \ldots, K_{22}^c \equiv K_{22}(x, x)$.

Equations (2.15) subject to the boundary condition (2.12) and appropriate initial conditions govern the evolution of a and b (and hence the dynamics of the flow through (2.5)) as long as no wave breaking is present; this is indeed the case if

$$a^2 + b^2 < \tfrac{1}{4} \tag{2.17}$$

throughout the flow field.

As discussed in KA, Long's steady flow (in the hydrostatic limit) corresponds to a particular steady-state solution of (2.15), $\bar{A} = \bar{a} + \mathrm{i}\bar{b}$, with no modulation in Y:

$$\bar{A}(x; \epsilon) = \bar{a} - \mathrm{i}\,\mathscr{H}\{\bar{a}\}, \tag{2.18}$$

where

$$\mathscr{H}\{\bar{a}\} = \frac{1}{\pi}\int_{-\infty}^{\infty} \frac{\bar{a}(s)}{s - x}\mathrm{d}s$$

stands for the Hilbert transform of $\bar{a}$. Imposing the boundary condition (2.12) then determines $\bar{a}(x; \epsilon)$ through the integral equation

$$\bar{a}\cos \epsilon f + \mathscr{H}\{\bar{a}\}\sin \epsilon f = -\tfrac{1}{2}\epsilon f. \tag{2.19}$$

As the topography amplitude is increased, there generally is a critical value of ϵ above which $\overline{A}$ is such that condition (2.17) is violated, so Long's steady flow features density inversions and flow reversals. In this study, attention is confined to the algebraic mountain (also known as the 'Witch of Agnesi'),

$$f(x) = \frac{1}{1+x^2},$$

for which this critical overturning amplitude is $\epsilon = 0.85$ (Miles & Huppert 1969).

3. Stability analysis

The goal now is to examine the stability of Long's steady flow in the hydrostatic limit on the basis of the asymptotic theory. To this end, we write

$$\psi^{(0)} = \overline{\psi} + \widetilde{\psi}, \qquad A = \overline{A}(x;\epsilon) + \widetilde{A}(x, Y, T), \tag{3.1}$$

where $\overline{A}$ corresponds to Long's hydrostatic steady state $\overline{\psi}(x, y)$, as obtained from (2.5), (2.18) and (2.19), and $\widetilde{A} = \widetilde{a} + \mathrm{i}\widetilde{b}$ to a small perturbation $\widetilde{\psi}(x, y, T)$. Substituting (3.1) into (2.15) and linearizing, the perturbation equations are

$$\overline{K}^c_{11}\widetilde{a}_T + \overline{K}^c_{12}\widetilde{b}_T + \widetilde{b}_{xY} + \int_{-\infty}^{x} \mathrm{d}x' \left(\overline{K}_{11x}\widetilde{a}'_T + \overline{K}_{12x}\widetilde{b}'_T\right) = 0, \tag{3.2a}$$

$$\overline{K}^c_{21}\widetilde{a}_T + \overline{K}^c_{22}\widetilde{b}_T - \widetilde{a}_{xY} + \int_{-\infty}^{x} \mathrm{d}x' \left(\overline{K}_{21x}\widetilde{a}'_T + \overline{K}_{22x}\widetilde{b}'_T\right) = 0, \tag{3.2b}$$

where the kernels are evaluated in terms of the known steady state (as indicated by the overbar). Moreover, the boundary condition (2.12) yields

$$\widetilde{a}\cos\epsilon f - \widetilde{b}\sin\epsilon f = 0 \qquad (Y = 0). \tag{3.3}$$

Some insight into the stability problem is gained by looking at the behaviour of perturbations at a long distance from the topography ($x \to \pm\infty$). In this limit, Long's steady flow approaches a uniform stream ($\overline{a},\ \overline{b} \to 0$), so $\overline{K}^c_{11},\ \overline{K}^c_{22} \to 1$ and $\overline{K}^c_{12},\ \overline{K}^c_{21} \to 0$ while the x-derivatives of the kernels go to zero. Consequently, equations (3.2) and the boundary condition (3.3) reduce to

$$\widetilde{a}_T + \widetilde{b}_{xY} = 0, \qquad \widetilde{b}_T - \widetilde{a}_{xY} = 0 \tag{3.4a,b}$$

and

$$\widetilde{a} = 0 \qquad (Y = 0). \tag{3.5}$$

This simplified system admits separable solutions,

$$\widetilde{a} = \sin mY\, \exp(\mathrm{i}\xi x + \sigma T), \qquad \widetilde{b} = \cos mY\, \exp(\mathrm{i}\xi x + \sigma T), \tag{3.6}$$

where m is real and $\sigma = \mathrm{i}m\xi$. These modes correspond to internal-wave disturbances on a uniformly stratified stream over a flat rigid bottom; they are neutral propagating waves if ξ is real and unstable evanescent waves if ξ is complex.

Returning now to the full stability problem (3.2), (3.3), note that, even though neither T nor Y appears explicitly in equations (3.2) ($\overline{K}_{11}, \ldots, \overline{K}_{22}$ depend on x alone), only the time dependence can be separated out; this complication arises from the boundary condition (3.3) on $Y = 0$ and is a consequence of the fact that Long's steady flow is not parallel for finite topography amplitude. Accordingly, we consider normal-mode disturbances proportional to $\exp(\sigma T)$ that are not separable in Y. As

$x \to \pm\infty$, however, each of these modes may be expressed in terms of the (complete) set of separable solutions (3.6). Therefore, an unstable mode (Re $\sigma > 0$) consists of evanescent waves ($\xi = -\mathrm{i}\sigma/m$ is complex) both far upstream and downstream, and a necessary condition for instability is the existence of modes that are trapped† over the topography (i.e. decay to zero as $x \to \pm\infty$).

On physical grounds, it is expected that no trapped modes exist when the topography is mild ($\epsilon \ll 1$) and the background flow deviates only slightly from a uniform stream. On the other hand, it would be interesting to know whether such modes become possible above a certain finite value of ϵ less than the critical overturning amplitude; in such a case, Long's steady flow would be unstable to modulations before static instability sets in.

This question is addressed by first looking for trapped modes of the stability equations (3.2) alone, ignoring the boundary condition (3.3), so the dependence on both T and Y can be separated out. It is then demonstrated that the critical value of ϵ for modulational instability obtained from this simplified modal analysis is somewhat lower than the critical topography amplitude predicted on the basis of the full stability problem (see §4).

We now seek separable normal-mode solutions of equations (3.2):

$$\begin{Bmatrix} \tilde{a} \\ \tilde{b} \end{Bmatrix} = \mathrm{Re} \begin{Bmatrix} \mathscr{A}(x) \\ \mathscr{B}(x) \end{Bmatrix} \mathrm{e}^{\mathrm{i}mY}\, \mathrm{e}^{\lambda m T}, \tag{3.7}$$

where m is the (real) vertical wavenumber and $\sigma = \lambda m$ is the possibly complex growth rate. The system (3.2) is then transformed to

$$\overline{K}^c_{11}\mathscr{A} + \overline{K}^c_{12}\mathscr{B} - \mathrm{i}\frac{1}{\lambda}\mathscr{B}_x + \int_{-\infty}^{x} \mathrm{d}x' \left(\overline{K}_{11x}\mathscr{A}' + \overline{K}_{12x}\mathscr{B}'\right) = 0, \tag{3.8a}$$

$$\overline{K}^c_{21}\mathscr{A} + \overline{K}^c_{22}\mathscr{B} + \mathrm{i}\frac{1}{\lambda}\mathscr{A}_x + \int_{-\infty}^{x} \mathrm{d}x' \left(\overline{K}_{21x}\mathscr{A}' + \overline{K}_{22x}\mathscr{B}'\right) = 0. \tag{3.8b}$$

Furthermore, at a long distance from the topography, it follows from (3.4) that

$$\begin{Bmatrix} \mathscr{A} \\ \mathscr{B} \end{Bmatrix} \sim \begin{Bmatrix} 1 \\ \pm\mathrm{i} \end{Bmatrix} \mathrm{e}^{\pm\lambda x} \qquad (|x| \to \infty). \tag{3.9}$$

We thus have an eigenvalue problem for $\mathscr{A}(x)$ and $\mathscr{B}(x)$ with a possibly 'mixed' spectrum: for purely imaginary values of the eigenvalue parameter λ, equations (3.8) have solutions that correspond to neutrally stable radiating waves according to (3.7), (3.9) for all ϵ. Apart from this continuous spectrum, however, when ϵ exceeds a certain critical value, there may exist a discrete spectrum comprising a finite number of complex eigenvalues (if λ is an eigenvalue so is $-\lambda^*$) for which $\mathscr{A}(x)$ and $\mathscr{B}(x)$ decay exponentially as $|x| \to \infty$ and correspond to trapped modes; hence, the existence of a discrete spectrum is a necessary condition for instability.

A search for trapped modes was made by numerically solving equations (3.8), subject to the boundary conditions

$$\mathscr{A}(x) \to 0 \quad (x \to \infty), \qquad \mathscr{B}(x) \to 0 \quad (x \to -\infty). \tag{3.10}$$

The numerical procedure uses finite differences on a non-uniform grid, allowing for

† These modes are distinct from the ones described by Laprise & Peltier (1989*a*) as trapped: in that study, the modes were trapped in the vertical direction between the ground and the steepest streamline.

finer resolution close to the topography. The derivatives $\mathscr{A}_x$ and $\mathscr{B}_x$ are evaluated by first-order forward and backward differences respectively, and the boundary conditions (3.10) are imposed at the ends of the computational domain. The hydrostatic Long's steady state is determined from (2.18), (2.19) using the procedure described by Lilly & Klemp (1979), and the kernels are computed as follows. Based on the assumption that there is no breaking streamline, $y = y(\psi^{(0)}; a, b,)$ is first determined by inverting (2.5) numerically using Newton–Raphson iteration; all the quantities in the integrals over $\psi^{(0)}$ for the kernels (2.16) are then known as functions of $(\psi^{(0)}; a, b)$ and the integrals are evaluated by the trapezoidal rule. The x-derivatives of the kernels are evaluated using centred differences. Finally, the integrals in (3.8) are computed using the trapezoidal rule.

This leads to a standard generalized matrix eigenvalue problem,

$$[C]\{z\} = \lambda[E]\{z\}.$$

Estimates of the spectrum were first generated for several topography amplitudes using a global eigenvalue solver, to obtain a rough approximation to the critical value of ϵ and the discrete eigenvalues. More refined approximations to these eigenvalues were then found by inverse iteration with shifting.

The real part of the most unstable (discrete) eigenvalue is plotted as a function of ϵ in figure 1. Indeed, there is a critical value of ϵ, less than the overturning amplitude $\epsilon = 0.85$, above which trapped modes become possible. The mode shapes $\mathscr{A}(x)$ and $\mathscr{B}(x)$ (normalized such that $\mathscr{A} = 1$ where $|\mathscr{A}|$ attains its maximum) for the case $\epsilon = 0.7$ are plotted in figure 2. Both the real and imaginary parts are clearly trapped close to the topography and they exhibit significant structure, especially on the upstream side of the obstacle. The scale over which the trapping occurs decreases rapidly with ϵ. Close to conditions at which instability sets in, the unstable modes are barely trapped, and determining the critical value of ϵ accurately is difficult. On the basis of figure 1, by extrapolation, we estimate that instability occurs for topography amplitudes above $\epsilon \approx 0.55$.

In terms of these trapped modes, it is straightforward to construct more general solutions to the perturbation equations (3.2) that represent locally confined unstable disturbances. For example, choosing a Gaussian distribution of vertical wavenumber m, superposition of the modes (3.7) yields

$$\begin{Bmatrix} \tilde{a} \\ \tilde{b} \end{Bmatrix} = \mathrm{Re}\left\{ \begin{matrix} \mathscr{A}(x) \\ \mathscr{B}(x) \end{matrix} \right\} \int_{-\infty}^{\infty} \mathrm{d}m\, \mathrm{e}^{\lambda m T}\, \mathrm{e}^{-m^2/4}\, \mathrm{e}^{-\mathrm{i}mY}. \tag{3.11}$$

It then follows that

$$\begin{Bmatrix} \tilde{a} \\ \tilde{b} \end{Bmatrix} \propto \mathrm{e}^{\lambda_r^2 T^2} \exp\left(-(\lambda_i T - Y)^2\right) \mathrm{Re}\left\{ \begin{matrix} \mathscr{A}\mathrm{e}^{\mathrm{i}\phi} \\ \mathscr{B}\mathrm{e}^{\mathrm{i}\phi} \end{matrix} \right\},$$

where $\lambda = \lambda_r + \mathrm{i}\lambda_i$ and $\phi = 2\lambda_r T(\lambda_i T - Y)$. It may be shown that the kinetic energy of this perturbation grows like $\exp(2\lambda_r^2 T^2)$ at large T, so the flow can be violently unstable when ϵ exceeds the critical value above which trapped modes exist.

Expression (3.11) was also used to check the results of the modal analysis by imposing on Long's steady state an initial disturbance that is Gaussian in Y and whose variation along x is given by the calculated trapped eigenmode. Using the numerical method outlined in the next section, this perturbation was then tracked in time and the result was found to agree very well with (3.11), verifying the computed modes and eigenvalues.

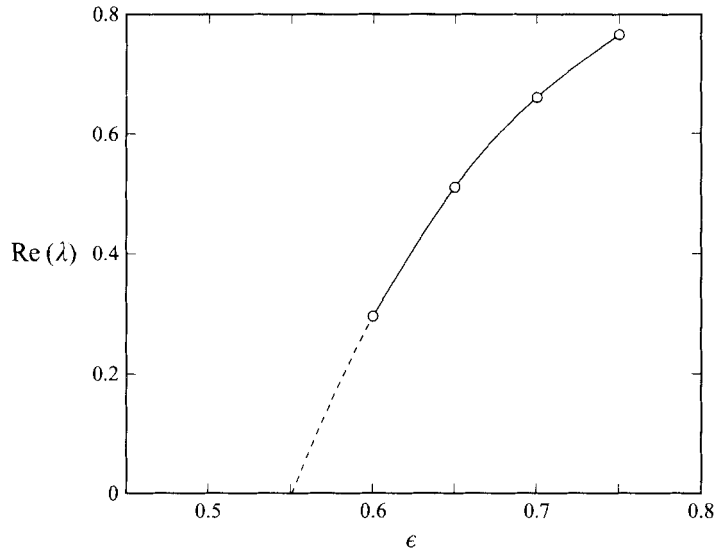

FIGURE 1. The real part of the most unstable eigenvalue λ of the discrete spectrum (corresponding to a trapped mode) as a function of ϵ.

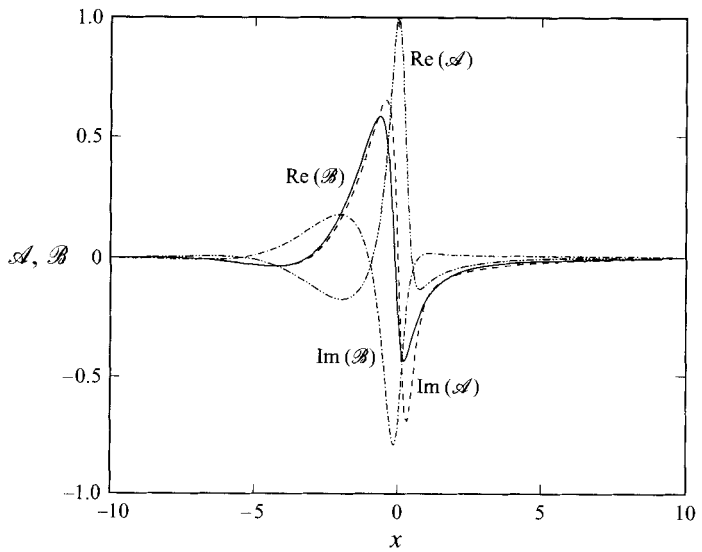

FIGURE 2. The dependence of the mode shapes $\mathscr{A}$ and $\mathscr{B}$ on x when $\epsilon = 0.7$. The trapping of the modes in the streamwise direction is evident.

The critical topography amplitude for modulational instability ($\epsilon \approx 0.55$) deduced from modal analysis of equations (3.2) is well below the critical overturning amplitude $\epsilon = 0.85$. As already noted, however, the separable modes (3.7) are not consistent with the boundary condition (3.3) on the topography; moreover, it is not clear that they can be combined to satisfy (3.3) by superposition.

To examine the influence of the wall on the threshold for modulational instability, one may compute trapped modes of the full stability problem (3.2), (3.3). The associated eigenvalue problem is not separable in Y, however, and extensive numerical

work is needed. Instead, we shall follow a more direct approach and solve (3.2), (3.3) numerically as an initial-value problem for a locally confined initial disturbance.

4. Evolution of a localized perturbation

4.1. *Energy budget*

In tracking the development of a disturbance numerically, it is useful to monitor the energetics of the flow. This is achieved by means of an energy-balance equation which also adds to the understanding of the instability mechanism by bringing out the energy exchange between the perturbation and the background steady flow.

To derive the desired equation for the energy of the perturbation, we write the flow variables as the sum of a steady mean representing Long's hydrostatic steady flow and a time-dependent small perturbation:

$$\boldsymbol{u} = \bar{\boldsymbol{u}} + \tilde{\boldsymbol{u}}, \qquad \rho = \bar{\rho} + \tilde{\rho}, \qquad p = \bar{p} + \tilde{p}.$$

Upon substitution into the equations of motion (2.1)–(2.3), invoking the Boussinesq approximation ($\beta \to 0$), and linearizing, the following perturbation equations are obtained in the hydrostatic limit ($\mu \to 0$):

$$\nabla \cdot \tilde{\boldsymbol{u}} = 0, \tag{4.1}$$

$$\tilde{\rho}_t + \bar{\boldsymbol{u}} \cdot \nabla \tilde{\rho} + \tilde{\boldsymbol{u}} \cdot \nabla \bar{\rho} = 0, \tag{4.2}$$

$$\tilde{\boldsymbol{u}}_t + \bar{\boldsymbol{u}} \cdot \nabla \tilde{u} + \tilde{\boldsymbol{u}} \cdot \nabla \bar{u} = -\frac{1}{\beta} \tilde{p}_x, \tag{4.3a}$$

$$\tilde{\rho} = -\tilde{p}_y, \tag{4.3b}$$

where $\bar{\boldsymbol{u}} = (\bar{u}, \bar{v})$ and $\tilde{\boldsymbol{u}} = (\tilde{u}, \tilde{v})$.

Now, multiplying (4.3a) with $\tilde{u}$, (4.3b) with $\tilde{v}/\beta$ and adding, using (4.1), one has

$$\tfrac{1}{2}(\tilde{u}^2)_t + \tfrac{1}{2}\nabla \cdot (\bar{\boldsymbol{u}} \tilde{u}^2) + \tilde{u}(\tilde{u}\bar{u}_x + \tilde{v}\bar{u}_y) + \frac{1}{\beta}(\tilde{\rho}\tilde{v} + \nabla \cdot (\tilde{p}\tilde{\boldsymbol{u}})) = 0.$$

Intergrating this equation over the entire fluid domain ($-\infty < x < \infty$, $\epsilon f < y < \infty$) and using the boundary conditions (the normal velocity must vanish on $y = \epsilon f$ and the perturbations vanish at infinity) then yields

$$\frac{\mathrm{d}}{\mathrm{d}t}(\mathrm{KE} + \mathrm{PE}) = \mathscr{R}, \tag{4.4}$$

where

$$\frac{\mathrm{d}}{\mathrm{d}t}\mathrm{KE} = \frac{1}{2}\frac{\mathrm{d}}{\mathrm{d}t}\int_{-\infty}^{\infty} \mathrm{d}x \int_{\epsilon f}^{\infty} \mathrm{d}y\, \tilde{u}^2$$

is the rate of change of the kinetic energy of the perturbation and

$$\frac{\mathrm{d}}{\mathrm{d}t}\mathrm{PE} = \frac{1}{\beta}\int_{-\infty}^{\infty} \mathrm{d}x \int_{\epsilon f}^{\infty} \mathrm{d}y\, \tilde{\rho}\tilde{v}$$

is the rate of change of the potential energy of the perturbation. The term on the right-hand side of (4.4),

$$\mathscr{R} = -\int_{-\infty}^{\infty} \mathrm{d}x \int_{\epsilon f}^{\infty} \mathrm{d}y\, \tilde{u}(\tilde{u}\bar{u}_x + \tilde{v}\bar{u}_y),$$

is the rate of work done by the Reynolds stresses. Depending on the sign of this term, power flows either from the mean flow to the perturbation or in the opposite direction.

Returning now to the asymptotic theory, equation (4.4) translates into an equivalent energy-balance equation in terms of the envelope variables. Specifically, with the same notation as in (3.1), one has to leading order in μ (consistent with the evolution equations (3.2) and the boundary condition (3.3))

$$\frac{\mathrm{d}}{\mathrm{d}t}\mathrm{KE} = \frac{\mathrm{d}}{\mathrm{d}T}\left\langle \tilde{a}^2 + \tilde{b}^2 \right\rangle, \tag{4.5a}$$

$$\frac{\mathrm{d}}{\mathrm{d}t}\mathrm{PE} = -\frac{1}{2\pi}\left\langle \int_{-\infty}^{x} \mathrm{d}x' \int_0^{2\pi} \mathrm{d}\overline{\psi}\left(\tilde{a}_x y_{\bar{a}} + \tilde{b}_x y_{\bar{b}}\right)\left(\tilde{a}'_T y'_{\bar{a}} + \tilde{b}'_T y'_{\bar{b}}\right)\right\rangle, \tag{4.5b}$$

where

$$\langle\cdot\rangle \equiv \int_{-\infty}^{\infty} \mathrm{d}x \int_0^{\infty} \mathrm{d}Y\,(\cdot).$$

Similarly, the power-input term on the right-hand side of (4.4) takes the form

$$\mathscr{R} = -2\epsilon \int_{-\infty}^{\infty} \mathrm{d}x f_x \left(\tilde{a}\sin\epsilon f + \tilde{b}\cos\epsilon f\right)^2\Big|_{Y=0} + \langle P(x, Y, T)\rangle, \tag{4.5c}$$

where

$$P = \frac{1}{2\pi}\int_0^{2\pi} \mathrm{d}\overline{\psi}\,\overline{\psi}_y \overline{H}\left\{\left(\tilde{a}_x\bar{b} - \tilde{b}\bar{a}_x\right) y_{\bar{a}}^2 + \left(\tilde{a}\bar{b}_x - \bar{a}\tilde{b}_x\right) y\frac{2}{b} - \left(\tilde{a}_x\bar{a} - \tilde{b}\tilde{b}_x - \tilde{a}\bar{a}_x + \tilde{b}\bar{b}_x\right) y_{\bar{a}} y_{\bar{b}}\right\}$$

and

$$\overline{H} = -\frac{\partial}{\partial\overline{\psi}}\int_{-\infty}^{x} \mathrm{d}x' y'\left(\tilde{a}'_T y'_{\bar{a}} + \tilde{b}'_T y'_{\bar{b}}\right) - \int_{-\infty}^{x} \mathrm{d}x'\left(\tilde{a}'_T y'_{\bar{a}} + \tilde{b}'_T y'_{\bar{b}}\right) + y\frac{\partial}{\partial\overline{\psi}}\int_{-\infty}^{x} \mathrm{d}x'\left(\tilde{a}'_T y'_{\bar{a}} + \tilde{b}'_T y'_{\bar{b}}\right).$$

Details of deriving expressions (4.5) are given in Appendix A.

In particular, when the topography amplitude is small ($\epsilon \ll 1$), it follows from (4.5*a*, *b*) that

$$\frac{\mathrm{d}}{\mathrm{d}t}\mathrm{PE} \sim \frac{\mathrm{d}}{\mathrm{d}t}\mathrm{KE},$$

while $\mathscr{R}$ is negligible according to (4.5*c*), to leading order. Hence, (4.4) implies that

$$\frac{\mathrm{d}}{\mathrm{d}T}\left\langle \tilde{a}^2 + \tilde{b}^2 \right\rangle = 0,$$

consistent with the simplified problem (3.4), (3.5).

4.2. *Numerical solution*

We next turn our attention to the numerical treatment of the initial-value problem for the evolution of a perturbation. Equations (3.2) are discretized by an explicit finite-difference method combined with Euler forward time stepping. A grid with non-uniform spacing in both x and Y is used to capture the details of the disturbance close to the topography. The kernels are evaluated numerically as described in §3,

taking great care to ensure that they are well resolved by the grid. All spatial derivatives are computed to second-order accuracy and the integrals are evaluated by the trapezoidal rule.

At each time step, the computation is commenced on $j = 1$, where j denotes the grid node number along Y, $j = 0$ corresponding to the boundary $Y = 0$. Using the simplified equations (3.4) that are valid far upstream, the values of $\tilde{a}$ and $\tilde{b}$ at the left boundary are determined first, and the entire (x, Y) plane ($j \geqslant 1$) is then covered by consecutive x-sweeps. Numerical-stability constraints dictate that the boundary condition (3.3) be applied on $j = 0$ by an implicit method: by evaluating on $j = 1$ the terms involving $\tilde{a}_{xY}$ and $\tilde{a}_T$, $\tilde{a}|_{j=0}$ is eliminated from (3.2*b*), and the resulting tridiagonal system is solved to obtain $\tilde{b}|_{j=0}$; the boundary condition (3.3) is then used to calculate $\tilde{a}|_{j=0}$. Despite the fact that this procedure was numerically stable for moderate values of ϵ, small grid-scale oscillations were observed along Y when ϵ was increased beyond 0.6 or so. Since this instability appeared to be very gentle, it was eliminated by using the 5-point smoothing stencil described by Shapiro (1975):

$$f_j = \tfrac{1}{16}(-f_{j-2} + 4f_{j-1} + 10f_j + 4f_{j+1} - f_{j+2}).$$

In a typical run of 2000 time steps, smoothing was applied every 100 steps. Moreover, the results were found to be virtually unaffected by cutting by half the number of times that smoothing was performed.

In implementing the above numerical procedure, the grid size used close to the topography varied from $\Delta X = 0.1$, $\Delta Y = 0.1$ for $\epsilon \leqslant 0.6$ to $\Delta X = 0.025$, $\Delta Y = 0.1$ for $\epsilon = 0.75$. The time step ΔT was chosen according to the stability condition $\Delta T \leqslant 0.1\ (\Delta X\ \Delta Y)$. Also, the finite computational domain was expanded as time increased to accommodate the spreading of the disturbance. This was done by monitoring the amplitudes $\tilde{a}$ and $\tilde{b}$ a few nodes away from the ends of the grid and adding a few points when the amplitudes exceeded a specified tolerance. The values of the amplitudes were set to zero at the ends of the grid. As a check of the accuracy of the numerical solution, the error in the energy budget (4.4) was typically less than 2%. Further details of the computational procedure are given in Ramirez (1993).

4.3. *Results*

Computations were carried out for several values of ϵ using the initial conditions

$$\tilde{a} = a_0 \exp(-(x^2 + Y^2)), \quad \tilde{b} = a_0 \exp(-(x^2 + Y^2)) \tan \epsilon f \qquad (T = 0), \tag{4.6}$$

a_0 being a normalization constant such that the kinetic energy of the disturbance $\langle \tilde{a}^2 + \tilde{b}^2 \rangle = 1$ at $T = 0$. This choice of initial disturbance is consistent with the boundary condition (3.3) and has its maximum close to the topography so the influence of the boundary on the stability characteristics is fully taken into account.

At low values of ϵ, the flow is stable, as expected. There is little energy exchange between the perturbation and the background flow; the disturbance spreads out with time, more or less as predicted by the simplified system (3.4), (3.5) that ignores the presence of the topography. Figure 3(*a*) illustrates the energy budget (4.4) as a function of T for the moderately small value of $\epsilon = 0.5$. The rate of change of

---

FIGURE 3. The energy budget for a small perturbation to Long's steady state for the cases (*a*) $\epsilon = 0.5$, (*b*) $\epsilon = 0.65$ and (*c*) $\epsilon = 0.7$. The circles and squares represent the rates of change of potential and kinetic energy respectively, while the triangles represent the rate of energy transfer from the mean flow to the perturbation.

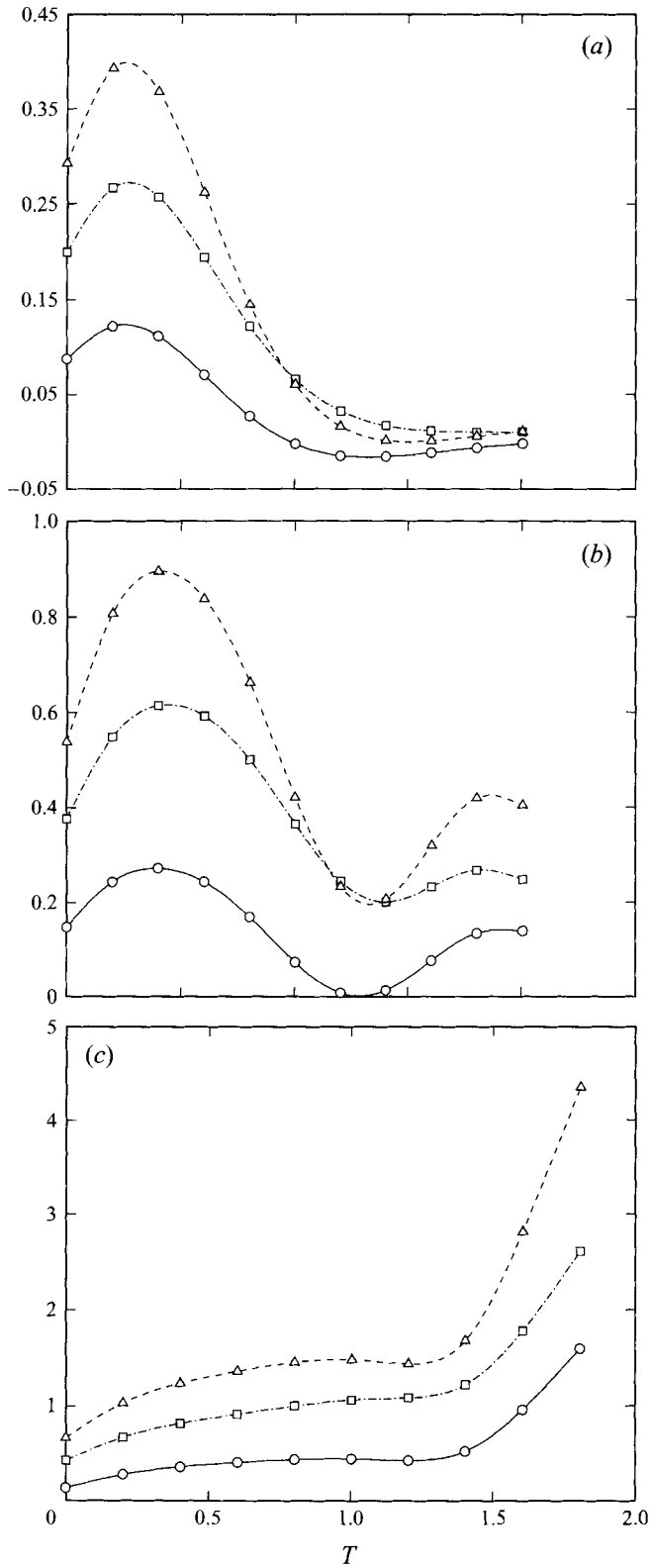

FIGURE 3. For caption see facing page.

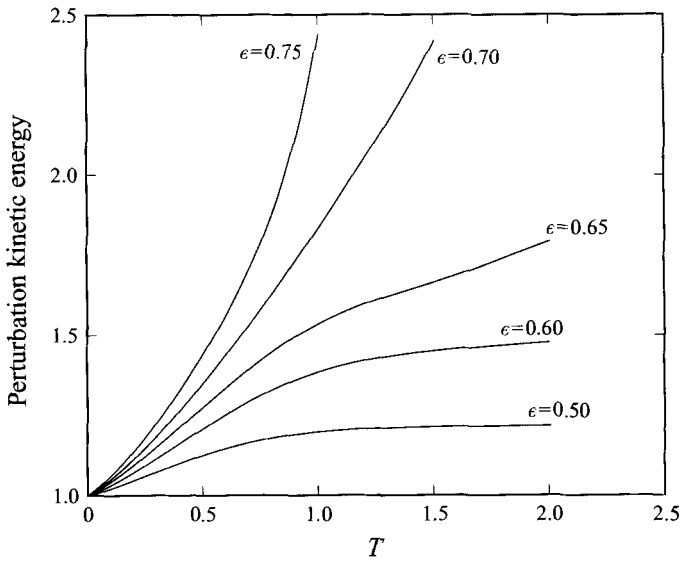

FIGURE 4. The perturbation kinetic energy as a function of T at various ϵ.

energy (potential and kinetic) of the perturbation increases from a positive value at $T = 0$ during the short time that most of the disturbance is still over the topography and can extract energy from the mean flow; at later times, when the disturbance has spread out, the energy budget exhibits a strongly damped oscillatory behaviour and the growth rate of the energy eventually decays to zero. This is also reflected in figure 4, where the kinetic energy of the disturbance is plotted as a function of T for several values of ϵ: for $\epsilon = 0.5$, the kinetic energy increases for a brief period of time and then approaches a constant value as the interaction with the mean flow ceases.

As the value of ϵ is increased, figure 4 shows that the kinetic energy of the perturbation grows for longer time, and there is a critical value of ϵ above which the energy appears to be growing indefinitely so the disturbance becomes unstable; the critical topography amplitude for instability appears to lie between $\epsilon = 0.6$ and $\epsilon = 0.65$. For values of ϵ in this transcritical range, the energy budget, as shown in figure 3(b) for $\epsilon = 0.65$, exhibits strong oscillations, the two opposing effects of spreading and energy extraction from the mean flow being more or less in balance.

In the unstable régime, on the other hand, the growth rates of the potential and kinetic energies of the perturbation eventually increase monotonically with time, as shown in figure 3(c) for $\epsilon = 0.7$. The power extracted from the mean flow by the perturbation also grows monotonically; hence, the perturbation grows at the expense of the mean flow. This continual energy transfer is facilitated by effectively trapping the disturbance over the topography, where the streamlines of the mean flow are most steep and the action of the Reynolds stress is most pronounced.

It was noted earlier (see (4.5a)) that $\langle|\widetilde{A}|^2\rangle = \langle\widetilde{a}^2 + \widetilde{b}^2\rangle$ measures the perturbation kinetic energy, so $|\widetilde{A}|^2$ may be interpreted as (averaged) kinetic energy density. To illustrate the significance of trapping in the instability mechanism, $|\widetilde{A}|^2$ is plotted in figure 5 as a function of x and Y at $T = 1.0$ for $\epsilon = 0.5$ and $\epsilon = 0.75$. At $T = 0$, $\langle|\widetilde{A}|^2\rangle = 1$ for both values of ϵ according to (4.6) and the initial conditions are similar. At $T = 1.0$, however, there are marked differences between the two disturbances: when no modulational instability is present ($\epsilon = 0.5$), the evolution is

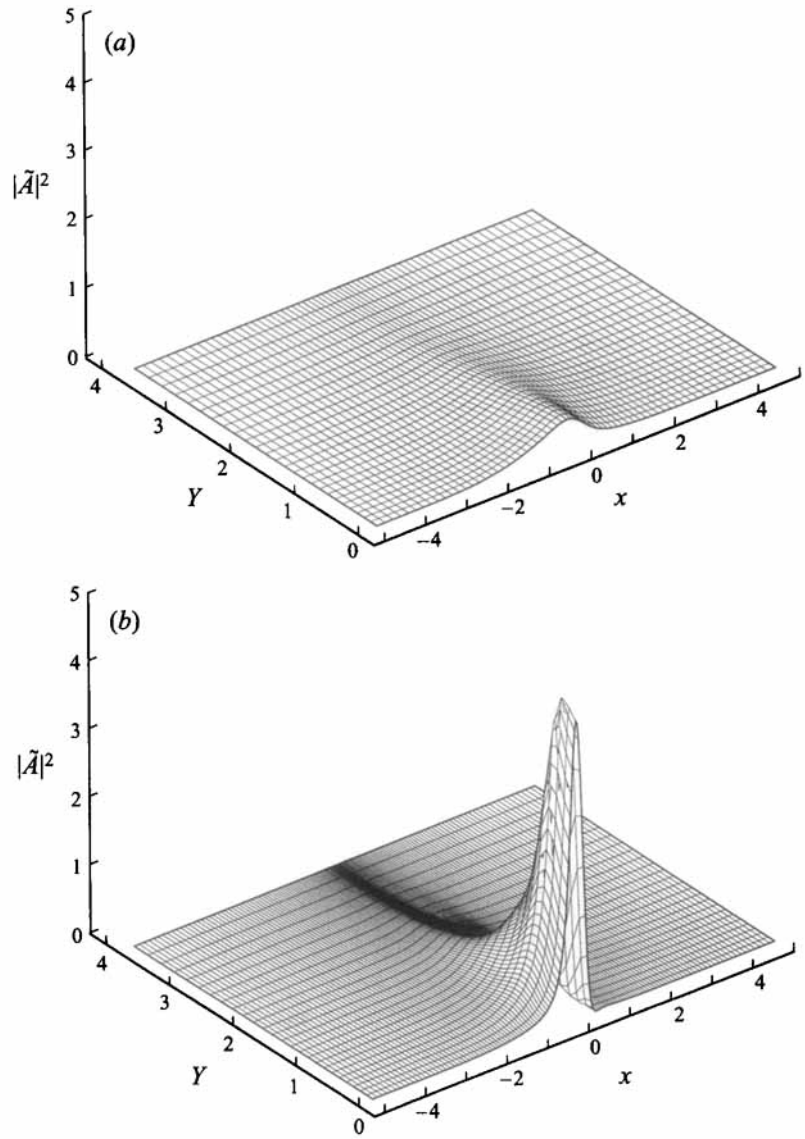

FIGURE 5. Perturbation kinetic energy density, $|\tilde{A}|^2$, as a function of x and Y at $T = 1.0$ for (*a*) $\epsilon = 0.5$ and (*b*) $\epsilon = 0.75$, illustrating the contrast between the spreading and trapping mechanisms.

dominated by spreading of the initial disturbance, while in the unstable case $\epsilon = 0.75$ the rapid growth of the perturbation close to the topography overwhelms spreading in the streamwise direction. This is consistent with the conclusion reached in §3 that a necessary condition for instability is the existence of trapped modes.

The critical topography amplitude for modulational instability obtained here, $\epsilon \approx 0.65$, is higher than the corresponding value of about 0.55 deduced from the modal analysis of equations (3.2) in §3. This difference must be attributed to the effect of the boundary condition (3.3) that is ignored in the modal analysis. To verify the role of the wall in inhibiting instability, we also tracked the evolution of an initial disturbance that was in the form (4.6) but was displaced from the boundary $Y = 0$

by a distance $Y_0 = 8$ such that the presence of the boundary took some time to be felt. For $\epsilon = 0.5$, which is well below critical in the presence of the boundary but is close to critical when the boundary is ignored, the energy budget (4.4) revealed a mild growth in the rate of change of the energy until the disturbance reached the boundary $Y = 0$ and this trend was reversed.

5. The transient problem

Based on the linear stability analysis presented above, Long's steady flow is unstable to infinitesimal modulations when the topography amplitude exceeds $\epsilon \approx 0.65$. Here we shall examine the transient development of the flow starting from rest, by solving the full nonlinear evolution equations (2.15), subject to the boundary condition (2.12), assuming that the topography is raised gradually to the specified amplitude. This way of establishing the flow mimics experimental conditions and avoids numerical difficulties associated with impulsive startup.

5.1. *Energy balance equation*

As in §4, we first derive an energy budget that will aid in verifying the accuracy of the computation and will also provide a global description of the flow field. Denoting by $\hat{\boldsymbol{u}} = (\hat{u}, \hat{v})$ the deviation of the velocity field from the uniform stream far upstream, and by $\hat{\rho}$ and $\hat{p}$ the deviations of the density and pressure, respectively, from their values far upstream, the governing equations (2.1)–(2.3) (in the hydrostatic limit $\mu \to 0$ and in the Boussinesq approximation $\beta \to 0$) take the form

$$\nabla \cdot \hat{\boldsymbol{u}} = 0, \tag{5.1}$$

$$\hat{\rho}_t + \hat{\rho}_x + \hat{\boldsymbol{u}} \cdot \nabla \hat{\rho} = 0, \tag{5.2}$$

$$\hat{u}_t + \hat{u}_x + \hat{\boldsymbol{u}} \cdot \nabla \hat{u} + \frac{1}{\beta} \hat{p}_x = 0, \tag{5.3a}$$

$$\hat{\rho} = -\hat{p}_y. \tag{5.3b}$$

Proceeding as before, combining the momentum equations (5.3) and using (5.1) yields

$$\tfrac{1}{2}(\hat{u}^2)_t + \tfrac{1}{2}(\hat{u}^2)_x + \tfrac{1}{2}\nabla \cdot (\hat{\boldsymbol{u}}\hat{u}^2) + \frac{1}{\beta}(\hat{\rho}\hat{v} + \nabla \cdot (\hat{p}\hat{\boldsymbol{u}})) = 0.$$

Upon integrating this equation over the fluid domain using the boundary conditions ($\hat{\boldsymbol{u}}$, $\hat{\rho}$ and $\hat{p}$ vanish in the far field and the component of velocity normal to the topography is zero), the following energy equation, analogous to (4.4), is obtained:

$$\frac{\mathrm{d}}{\mathrm{d}t}(\mathrm{KE} + \mathrm{PE}) = \mathscr{R}; \tag{5.4}$$

here, as in (4.4),

$$\frac{\mathrm{d}}{\mathrm{d}t}\mathrm{KE} = \frac{1}{2}\frac{\mathrm{d}}{\mathrm{d}t}\int_{-\infty}^{\infty} \mathrm{d}x \int_{\epsilon f}^{\infty} \mathrm{d}y\, \hat{u}^2$$

is the rate of change of kinetic energy and

$$\frac{\mathrm{d}}{\mathrm{d}t}\mathrm{PE} = \frac{1}{\beta}\int_{-\infty}^{\infty} \mathrm{d}x \int_{\epsilon f}^{\infty} \mathrm{d}y\, \hat{\rho}\hat{v}$$

is the rate of change of potential energy. The term on the right-hand side of (5.4),

$$\mathscr{R} = \frac{\epsilon}{\beta}\int_{-\infty}^{\infty} \mathrm{d}x f_x\, \hat{p}|_{y=\epsilon f},$$

however, has a somewhat different interpretation from the corresponding term in (4.4): it is the rate of energy imparted to the flow by the force that is responsible for establishing the motion. Alternatively, if the obstacle were being towed in a stratified fluid, this term would be the power required to tow the obstacle.

The energy-balance equation (5.4) may be expressed in terms of the envelope variables (see Appendix B); to leading order in μ, one has

$$\frac{\mathrm{d}}{\mathrm{d}t}\mathrm{KE} = \frac{\mathrm{d}}{\mathrm{d}T}\left\langle a^2 + b^2\right\rangle, \tag{5.5a}$$

$$\frac{\mathrm{d}}{\mathrm{d}t}\mathrm{PE} = -\frac{1}{2\pi}\left\langle \int_{-\infty}^{\infty}\mathrm{d}x' \int_0^{2\pi} \mathrm{d}\psi^{(0)}\left(a_x y_a + b_x y_b\right)\left(a'_T y'_a + b'_T y'_b\right)\right\rangle, \tag{5.5b}$$

$$\mathscr{R} = \epsilon\int_{-\infty}^{\infty}\mathrm{d}x f_x\left\{2\left(a\sin\epsilon f + b\cos\epsilon f\right)|_{Y=0} + \int_0^{\infty}\mathrm{d}Y\, Q(x, Y, T)\right\}, \tag{5.5c}$$

where

$$Q = \frac{1}{2\pi}\int_{-\infty}^{x}\mathrm{d}x'\int_0^{2\pi}\mathrm{d}\psi^{(0)}\frac{1}{\psi_y^{(0)}}\left\{a'_T\left(\left(y'y'_a\right)_{\psi^{(0)}} - yy'_{a\psi^{(0)}}\right) + b'_T\left(\left(y'y'_b\right)_{\psi^{(0)}} - yy'_{b\psi^{(0)}}\right)\right\}.$$

In the small-amplitude limit ($\epsilon \ll 1$), it follows from (5.5*a*, *b*) that

$$\frac{\mathrm{d}}{\mathrm{d}t}\mathrm{PE} \sim \frac{\mathrm{d}}{\mathrm{d}t}\mathrm{KE}.$$

Furthermore, (5.5*c*) gives

$$\mathscr{R} \sim 2\epsilon\int_{-\infty}^{\infty}\mathrm{d}x\, f_x\left(b - b^2\right)|_{Y=0}.$$

Hence, to leading order, (5.4) implies that

$$\frac{\mathrm{d}}{\mathrm{d}T}\left\langle a^2 + b^2\right\rangle \sim \epsilon\int_{-\infty}^{\infty}\mathrm{d}x\, f_x\left(b - b^2\right)|_{Y=0},$$

which may also be derived directly from the linearized versions of the evolution equations (2.15) and the boundary condition (2.12).

5.2. *Numerical method*

The overall strategy for solving the evolution equations (2.15) numerically parallels that described in §4 for the stability problem. A non-uniform grid with second-order approximation of the spatial derivatives by finite differences and forward Euler time stepping are used. One essential difference, however, is that the kernels here are no longer independent of T (and Y) but change as the flow evolves, and have to be updated at every time step over the entire grid; this makes the computation much more expensive.

In order to reduce the cost, the following procedure was adopted. According to (2.16), the kernels are functions of (a, b, a', b'). When $a^2 + b^2 + a'^2 + b'^2$ exceeded an upper threshold equal to 0.1, the kernels were evaluated numerically as in §4 whereas when this amplitude criterion was less than a lower threshold of 0.01, the linear limits $K_{11} = K_{22} = 1$, $K_{21} = K_{12} = 0$ were used. For intermediate values of the

amplitudes, the kernels were evaluated using an analytic approximation: equation (2.5) for the streamfunction $\psi^{(0)}$ was inverted in terms of a power series to determine $y = y(\psi^{(0)}; a, b)$ correct to eighth order in a and b. With this approximation of y and its derivatives inserted in (2.16), analytic expressions for the kernels, correct to sixth order in (a, b, a', b'), were obtained (Ramirez 1993). In a similar manner, the x-derivatives of the kernels were evaluated using

$$\frac{\partial}{\partial x}K_{mn}(x, x') = a_x \frac{\partial}{\partial a}K_{mn}(a, b, a', b') + b_x \frac{\partial}{\partial b}K_{mn}(a, b, a', b')$$

for $m, n = 1, 2$.

As in §4, the boundary condition (2.12) was applied implicitly: the values of b on the boundary $Y = 0 (j = 0)$ were determined from (2.15b) first (evaluating the kernels and the terms involving a_T and a_{xY} on $j = 1$) and then (2.12) was used to obtain a on $j = 0$; details may be found in Prasad (1996). The grid size used (close to the topography) varied from $\Delta X = \Delta Y = 0.1$ for $\epsilon \leqslant 0.65$ to $\Delta X = 0.025$, $\Delta Y = 0.1$ for the highest topography amplitude $\epsilon = 0.75$ that we considered; the time step ΔT satisfied the stability condition $\Delta T \leqslant 0.1 \Delta X \Delta Y$. Moreover, it was found necessary to apply smoothing in this case as well in order to eliminate a mild numerical instability along the vertical direction. Finally, the radiation condition was implemented by expanding the computational domain as before.

5.3. *Results*

The transient problem was solved for values of ϵ ranging from 0.5 to 0.75. The forcing was turned on according to

$$f(x, T) = \frac{1}{1 + x^2}(1 - \mathrm{e}^{-10T}),$$

so the topography achieved 99% of its maximum amplitude before $T = 0.5$. The results are presented in terms of the energy budget (5.4) and

$$d(x, T) \equiv \left(|A|^2_{Y=0} - |\overline{A}|^2\right) / |\overline{A}|^2_{max},$$

where $\overline{A}(x)$ is the envelope corresponding to Long's steady flow and $|\overline{A}|_{max}$ is the maximum value of $|\overline{A}|$. From the above definition, it is clear that $d(x, T)$ measures the local deviation of the transient flow from Long's steady state on the lower boundary.

The energy budget for $\epsilon = 0.5$ is shown in figure 6(a); the energy-balance equation (40) is satisfied to within 2%†. The rates of change of both the kinetic and potential energies as well as the external power input approach constant values shortly after the forcing has reached its maximum value, indicating that a steady state has been achieved. To check how close this steady state is to Long's steady flow, the quantity $d(x, T)$ is plotted in figure 6(b) as a function of x at three different times. As measured by d, the deviation from Long's steady state is quite small (about 3%) and varies little with time; moreover, d is more or less symmetric about $x = 0$ and decays rapidly to zero far from the topography at large T. Hence, it would seem that Long's steady state is achieved for $\epsilon = 0.5$. We recall that, for this value of ϵ, Long's steady state is stable to infinitesimal modulations, and nonlinearity does not turn out to have a destabilizing effect on the transient response.

When the topography amplitude is raised to a value of $\epsilon = 0.7$ for which the corresponding Long steady flow is linearly unstable, however, the energy budget is

† The error is larger during the time that the topography has not yet reached its maximum amplitude. This error can be reduced by turning on the topography more slowly.

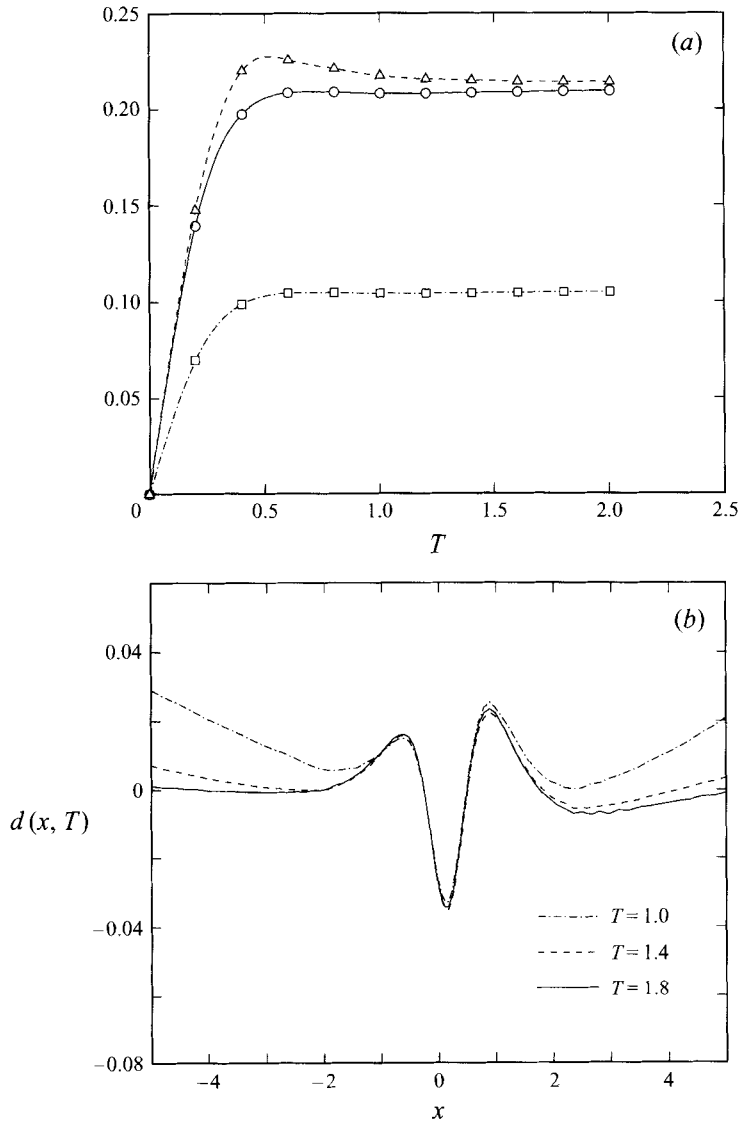

FIGURE 6. (*a*) The energy budget for the transient response with $\epsilon = 0.5$. The squares represent the rate of change of potential energy while the circles represent the rate of change of total energy; the triangles denote the power input to the flow. (*b*) The deviation parameter $d(x, T)$ as a function of x at $T = 1.0, 1.4$ and 1.8 for $\epsilon = 0.5$.

quite different in character. As shown in figure 7(*a*), the effect of nonlinearity here is to curtail the monotonic growth observed in the linear stability problem (figure 3*c*), resulting in what appears to be a sustained oscillation in the energy budget. The oscillation occurs on an $O(1)$ timescale in terms of $T = \mu^2 t$, so the period of oscillation ($T \approx 1.5$) is very long, $O(1/\mu^2)$, in terms of the convective timescale. The response, in turn, exhibits a slowly varying transient behaviour rather than reaching steady state. The quantity $d(x, T)$ that measures the deviation from Long's steady flow is plotted in figure 7(*b*) as a function of x at the same three times as in figure 6(*b*). While the values of d are still fairly small (on the order of 6–7%), they are

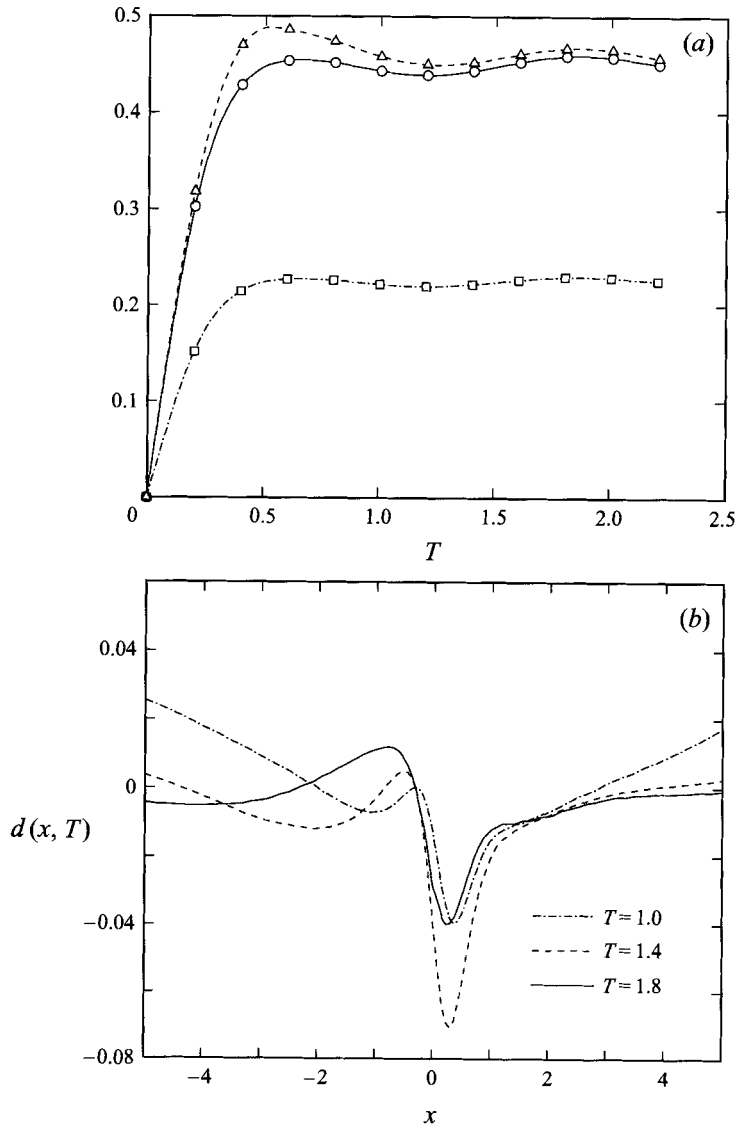

FIGURE 7. (*a*) The energy budget for the transient response with $\epsilon = 0.7$. The squares represent the rate of change of potential energy while the circles represent the rate of change of total energy; the triangles denote the power input to the flow. (*b*) The deviation parameter $d(x, T)$ as a function of x at $T = 1.0, 1.4$ and 1.8 for $\epsilon = 0.7$.

strongly dependent on T in view of the transient nature of the flow; hence, the flow is different from that at Long's steady state but not substantially so. We remark that this transient flow behaviour is qualitatively similar to that found by Lamb (1994) in the corresponding finite-depth problem for values of the topography amplitude for which no breaking occurs.

Comparing figure 7(*b*) with figure 6(*b*), it is also observed that in the case $\epsilon = 0.7$ where instability is present, the deviation of the transient reponse from Long's steady flow is markedly asymmetric about $x = 0$. Moreover, while the deviation downstream most likely goes to zero as T increases, this does not seem to be the case on the

upstream side. Whether or not, ultimately, this causes upstream influence is not clear and would require carrying the computation to much larger values of T in order to give a definitive answer. The amplitude of the upstream disturbance is quite small, however; certainly, there is no significant upstream influence comparable to that found near resonant flow conditions in the finite-depth problem (Grimshaw & Yi 1991).

The energy budget in figure 7(*a*) for $\epsilon = 0.7$ exhibits an overshoot shortly after the forcing achieves its maximum amplitude, followed by a dip. It therefore seemed possible that the overshoot might lead to transient breaking at larger subcritical values of the mountain amplitude. To check this hypothesis, an abbreviated calculation was performed for $\epsilon = 0.75$ up to $T = 1.2$. While the amplitude of the fluctuation about Long's steady flow increases, no evidence of transient breaking was found. Thus, if transient breaking does occur, it will most likely do so very close to the critical overturning amplitude of 0.85, consistent with the numerical results of Pierrehumbert & Bacmeister (1987). In conclusion, the modulational instability is rather mild in nature, causing the flow to go into a slowly varying transient state near Long's steady state without the occurrence of transient breaking.

6. Discussion

The present investigation has addressed the stability and realizability of Long's steady flow in the hydrostatic limit using the asymptotic theory of KA. For the algebraic mountain, this steady state is unstable to small-amplitude modulations for values of the topography steepness $\epsilon \gtrsim 0.65$, significantly below the critical overturning value of $\epsilon = 0.85$. This is clearly in contrast to the results of earlier investigations (Laprise & Peltier 1989*a*; Pierrehumbert & Wyman 1985; Clark & Peltier 1977), where it was found that the criteria for static and dynamic instabilities are simultaneously satisfied. These results are frequently justified by appealing to the Miles–Howard theorem, according to which the local Richardson number Ri has to be less than $\frac{1}{4}$ somewhere in the flow field for shear-flow instability to occur (Drazin & Reid 1981, p. 328), a condition that is first met at the critical amplitude for static instability (Lilly & Klemp 1979). However, it must be borne in mind that the above criterion applies to parallel flows, whereas the flows considered here (ϵ is finite) are strongly non-parallel, especially when the steepness approaches the critical value. This caveat of the Miles–Howard theorem has also been emphasized by Howard & Maslowe (1973) and the fact that $Ri < \frac{1}{4}$ at the critical steepness must therefore be regarded as fortuitous.

We have also demonstrated, using an eigenvalue analysis, that modes trapped near the topography in the streamwise direction must exist for instability to occur. Physically, this condition ensures that disturbances can lodge in the region where the background shear is maximum so they can draw energy from the mean flow continually.

The effects of this instability on the realizability of Long's steady flow were studied by means of a transient calculation starting from rest. The stability boundary was found to agree with that of the linear stability problem. In the unstable régime $\epsilon \gtrsim 0.65$, the effect of nonlinearity causes the transient flow to fluctuate in the neighbourhood of Long's steady state. The transients evolve slowly – on a timescale $T = O(1)$ representing a large number of convective time units – which could explain why the modulational instability passed unnoticed in previous work. For example, in Laprise & Peltier (1989*b*), the simulations for $\mu = 0.1$ with $\epsilon = 0.95$ (a supercritical

amplitude at which the authors found a dominant shear-flow instability) were carried out to 36 convective time units, corresponding to $T = 0.36$. The slow evolution of the response that we observe also supports the view that transient upstream motions could be mistaken for upstream influence at subcritical topography amplitudes.

We found no transient wave breaking even when ϵ was within 10% of the critical overturning value. We suspect that if subcritical transient breaking occurs, it must do so when the topography steepness is very close to the critical value predicted by Long's model. This is in stark contrast to the results found in the corresponding finite-depth problem where transient subcritical breaking is quite common (Grimshaw & Yi 1991; Lamb 1994).

Quantitative comparison of the present results with the experiments of Baines & Hoinka (1985) is difficult since their obstacles were significantly non-hydrostatic. We remark, however, that, according to Baines & Hoinka (1985), there is a range of moderately small topography amplitudes for which the flow does not reach steady state but develops slowly without breaking; moreover, in this régime, their data indicates the presence of small-amplitude upstream motions that they interpret as upstream influence (if viscous effects were neglected). It would seem that this flow behaviour resembles, at least qualitatively, the slowly varying transient response found here when modulational instability is present. However, in making a detailed comparison between theory and experiment, non-hydrostatic and viscous effects (that may cause flow separation, among other things) could play an important part.

Finally, we remark that when the flow is transient, the density perturbation does not decay to zero far downstream according to (2.9), but rather gives rise to an $O(\mu^2)$ columnar disturbance that persists in the streamwise direction and is modulated in the vertical direction. The appearance of a similar 'shelf' owing to transient effects was also noted by Warn (1983) in his study of large-amplitude Rossby waves in a fluid of finite depth. It then becomes necessary to treat the flow field far downstream separately by rescaling the equations to account for the evolution of the shelf in the streamwise direction. This problem is discussed in detail by Prasad (1996) in the context of three- dimensional stratified flows of finite depth, where the problems caused by the shelf are far more severe. It may be noted that a two-dimensional stratified flow of finite depth (Grimshaw & Yi 1991) also features a downstream shelf. However, the appearance of these shelves does not alter the results of either that study or the present one, except for the finer details of the downstream flow field.

This work was supported by the Air Force Office of Scientific Research Grant F49620-92-J-0086.

Appendix A. Energetics of small localized disturbance

Here we demonstrate how the energy-balance equation (4.4) for the evolution of a small localized disturbance to Long's steady state is expressed in terms of the scaled variables used in the asymptotic theory of KA.

We begin with the rate of change of kinetic energy

$$\frac{\mathrm{d}}{\mathrm{d}t}\mathrm{KE} = \frac{1}{2}\frac{\mathrm{d}}{\mathrm{d}t}\int_{-\infty}^{\infty}\mathrm{d}x\int_{\epsilon f}^{\infty}\mathrm{d}y\,\tilde{u}^2.$$

Since $\tilde{u} = \tilde{\psi}_y$ and

$$\tilde{\psi} = 2(\tilde{a}\cos y - \tilde{b}\sin y), \tag{A 1}$$

one has to leading order in μ

$$\int_{\epsilon f}^{\infty} \mathrm{d}y\, \tilde{\psi}_y^2 \sim \frac{2}{\mu^2} \int_0^{\infty} \mathrm{d}Y (\tilde{a}^2 + \tilde{b}^2).$$

Hence,

$$\frac{\mathrm{d}}{\mathrm{d}t}\mathrm{KE} = \frac{\mathrm{d}}{\mathrm{d}T} \left\langle \tilde{a}^2 + \tilde{b}^2 \right\rangle,$$

in agreement with (4.5*a*).

We next consider the rate of change of potential energy

$$\frac{\mathrm{d}}{\mathrm{d}t}\mathrm{PE} = \frac{1}{\beta} \int_{-\infty}^{\infty} \mathrm{d}x \int_{\epsilon f}^{\infty} \mathrm{d}y\, \tilde{\rho}\, \tilde{v},$$

where $\tilde{v} = -\tilde{\psi}_x$ and, from (2.9),

$$\tilde{\rho} = -\beta\tilde{\psi} + \mu^2\beta \int_{-\infty}^{x} \left. \frac{\tilde{\psi}_T}{\overline{\psi}_y} \right|_{\overline{\psi}} \mathrm{d}x'.$$

Therefore,

$$\frac{\mathrm{d}}{\mathrm{d}t}\mathrm{PE} = \tfrac{1}{2} \int_{-\infty}^{\infty} \mathrm{d}x \int_{\epsilon f}^{\infty} \mathrm{d}y\, (\tilde{\psi}^2)_x - \mu^2 \int_{-\infty}^{\infty} \mathrm{d}x \int_{\epsilon f}^{\infty} \mathrm{d}y\, \tilde{\psi}_x \int_{-\infty}^{x} \left. \frac{\tilde{\psi}_T}{\overline{\psi}_y} \right|_{\overline{\psi}} \mathrm{d}x'. \tag{A 2}$$

By integration by parts, invoking the boundary conditions (2.4) and (3.3), the first term above can be readily shown to vanish. Using then (A1) and

$$\overline{\psi} = y + 2\left(\bar{a}\cos y - \bar{b}\sin y\right), \tag{A 3}$$

the integrand of the second term in (A2) gives

$$\int_{\epsilon f}^{\infty} \mathrm{d}y\, \tilde{\psi}_x \int_{-\infty}^{x} \left. \frac{\tilde{\psi}_T}{\overline{\psi}_y} \right|_{\overline{\psi}} \mathrm{d}x'$$

$$\sim \frac{2}{\pi}\frac{1}{\mu^2} \int_0^{\infty} \mathrm{d}Y \int_{-\infty}^{x} \mathrm{d}x' \int_0^{2\pi} \mathrm{d}\overline{\psi}\, \frac{1}{\overline{\psi}_y \overline{\psi}'_y} \left(\tilde{a}_x \cos y - \tilde{b}_x \sin y\right) \left(\tilde{a}'_T \cos y' - \tilde{b}'_T \sin y'\right). \tag{A 4}$$

However, from (A3),

$$\sin y = \tfrac{1}{2}\, y_{\bar{b}}\, \overline{\psi}_y, \qquad \cos y = -\tfrac{1}{2}\, y_{\bar{a}}\, \overline{\psi}_y, \tag{A 5}$$

and combining (A2) with (A4) and (A5) yields (4.5*b*).

Finally, using (2.11), (A1) and (A3), the power-input term takes the form

$$\mathscr{R} = -\tfrac{1}{2}\epsilon \int_{-\infty}^{\infty} \mathrm{d}x f_x\, \tilde{\psi}_y^2\big|_{y=\epsilon f} - \mu^2 \left\{ \int_{-\infty}^{\infty} \mathrm{d}x \int_{\epsilon f}^{\infty} \mathrm{d}y \overline{H} \left(\mathrm{i}\tilde{\psi}_x \overline{A} - \tilde{\psi}_y \overline{A}_x\right) \mathrm{e}^{\mathrm{i}y} + \text{c.c.} \right\}, \tag{A 6}$$

where

$$\overline{H} = -\frac{\partial}{\partial\overline{\psi}} \int_{-\infty}^{x} \tilde{\psi}_{yT}|_{\overline{\psi}}\, \mathrm{d}x' + \frac{\partial}{\partial\overline{\psi}} \int_{-\infty}^{x} y \left. \frac{\tilde{\psi}_T}{\overline{\psi}_y} \right|_{\overline{\psi}} \mathrm{d}x' - y \frac{\partial}{\partial\overline{\psi}} \int_{-\infty}^{x} \left. \frac{\tilde{\psi}_T}{\overline{\psi}_y} \right|_{\overline{\psi}} \mathrm{d}x'.$$

Now, using (A1) and (A3), it follows that

$$\int_{\epsilon f}^{\infty} \mathrm{d}y \overline{H} \left(\mathrm{i}\tilde{\psi}_x \overline{A} - \tilde{\psi}_y \overline{A}_x\right) \mathrm{e}^{\mathrm{i}y} + \text{c.c.} \sim -\frac{1}{\mu^2} \int_0^{\infty} \mathrm{d}Y\, P(x, Y, T), \tag{A 7}$$

where

$$P = \frac{1}{2\pi}\int_0^{2\pi} \mathrm{d}\overline{\psi}\,\overline{\psi}_y\,\overline{H}\left\{\left(\widetilde{a}_x\overline{b} - \widetilde{b}\overline{a}_x\right)y_{\overline{a}}^2 + \left(\widetilde{a}\overline{b}_x - \widetilde{b}_x\overline{a}\right)y_{\overline{b}}^2 - \left(\widetilde{a}_x\overline{a} - \widetilde{b}_x\overline{b} - \widetilde{a}\overline{a}_x + \widetilde{b}\overline{b}_x\right)y_{\overline{a}}y_{\overline{b}}\right.$$

and

$$\overline{H} = -\frac{\partial}{\partial\overline{\psi}}\int_{-\infty}^{x}\mathrm{d}x'y'\left(\widetilde{a}'_T y'_{\overline{a}} + \widetilde{b}'_T y'_{\overline{b}}\right) - \int_{-\infty}^{x}\mathrm{d}x'\left(\widetilde{a}'_T y'_{\overline{a}} + \widetilde{b}'_T y'_{\overline{b}}\right) + y\frac{\partial}{\partial\overline{\psi}}\int_{-\infty}^{x}\mathrm{d}x'\left(\widetilde{a}'_T y'_{\overline{a}} + \widetilde{b}'_T y'_{\overline{b}}\right).$$

Combining then (A6) with (A7) yields (4.5*c*).

Appendix B. Energetics of transient response

Here we give details of the manipulation involved in expressing the energy-balance equation (5.4) for the transient response in terms of the scaled variables used in the asymptotic theory of KA.

The rate of change of kinetic energy is

$$\frac{\mathrm{d}}{\mathrm{d}t}\mathrm{KE} = \frac{1}{2}\frac{\mathrm{d}}{\mathrm{d}t}\int_{-\infty}^{\infty}\mathrm{d}x\int_{\epsilon f}^{\infty}\mathrm{d}y\,\hat{u}^2,$$

where $\hat{u} = \hat{\psi}_y$ and

$$\hat{\psi} = 2(a\cos y - b\sin y).$$

Therefore,

$$\int_{\epsilon f}^{\infty}\mathrm{d}y\,\hat{\psi}_y^2 \sim \frac{2}{\mu^2}\int_0^{\infty}\mathrm{d}Y\,(a^2+b^2),$$

and

$$\frac{\mathrm{d}}{\mathrm{d}t}\mathrm{KE} = \frac{\mathrm{d}}{\mathrm{d}T}\langle a^2+b^2\rangle$$

as in (5.5*a*).

We next consider the rate of change of potential energy

$$\frac{\mathrm{d}}{\mathrm{d}t}\mathrm{PE} = \frac{1}{\beta}\int_{-\infty}^{\infty}\mathrm{d}x\int_{\epsilon f}^{\infty}\mathrm{d}y\,\hat{\rho}\,\hat{v},$$

where $\hat{v} = -\hat{\psi}_x$ and, from (2.9),

$$\hat{\rho} = -\beta\hat{\psi} + \mu^2\beta\int_{-\infty}^{x}\left.\frac{\hat{\psi}_T}{\psi_y^{(0)}}\right|_{\psi^{(0)}}\mathrm{d}x'. \tag{B 1}$$

Therefore,

$$\frac{\mathrm{d}}{\mathrm{d}t}\mathrm{PE} = \tfrac{1}{2}\int_{-\infty}^{\infty}\mathrm{d}x\int_{\epsilon f}^{\infty}\mathrm{d}y\,(\hat{\psi}^2)_x - \mu^2\int_{-\infty}^{\infty}\mathrm{d}x\int_{\epsilon f}^{\infty}\mathrm{d}y\,\hat{\psi}_x\int_{-\infty}^{x}\left.\frac{\hat{\psi}_T}{\psi_y^{(0)}}\right|_{\psi^{(0)}}\mathrm{d}x'. \tag{B 2}$$

Upon integration by parts, the first term above becomes

$$\tfrac{1}{2}\int_{-\infty}^{\infty}\mathrm{d}x\int_{\epsilon f}^{\infty}\mathrm{d}y\,(\hat{\psi}^2)_x = \tfrac{1}{2}\epsilon\int_{-\infty}^{\infty}\mathrm{d}x\,f_x\,\hat{\psi}^2\big|_{y=\epsilon f},$$

and, invoking the boundary condition (2.12), this term vanishes. Furthermore,

$$\int_{\epsilon f}^{\infty} \mathrm{d}y\, \hat{\psi}_x \int_{-\infty}^{x} \left.\frac{\hat{\psi}_T}{\psi_y^{(0)}}\right|_{\psi^{(0)}} \mathrm{d}x'$$

$$\sim \frac{2}{\pi}\frac{1}{\mu^2}\int_0^{\infty}\mathrm{d}Y \int_{-\infty}^{x}\mathrm{d}x' \int_0^{2\pi}\mathrm{d}\psi^{(0)} \frac{1}{\psi_y^{(0)}\psi_y^{(0)\prime}}\,(a_x\cos y - b_x \sin y)(a_T'\cos y' - b_T'\sin y'). \tag{B 3}$$

Combining then (B2) with (B3), using

$$\sin y = \tfrac{1}{2} y_b \psi_y^{(0)}, \qquad \cos y = -\tfrac{1}{2} y_a \psi_y^{(0)}, \tag{B 4}$$

yields (5.5*b*).

Finally, from (5.3*b*),

$$\hat{p}|_{y=\epsilon f} = \int_{\epsilon f}^{\infty} \hat{\rho}\,\mathrm{d}y,$$

where $\hat{\rho}$ is given by (B1), and the rate of energy imparted to the flow takes the form

$$\mathscr{R} = -\epsilon \int_{-\infty}^{\infty}\mathrm{d}x\, f_x \int_{\epsilon f}^{\infty}\mathrm{d}y\,\hat{\psi} + \mu^2\epsilon\int_{-\infty}^{\infty}\mathrm{d}x\, f_x\int_{\epsilon f}^{\infty}\mathrm{d}y\int_{-\infty}^{x}\left.\frac{\hat{\psi}_T}{\psi_y^{(0)}}\right|_{\psi^{(0)}}\mathrm{d}x'. \tag{B 5}$$

In view of (2.11) and (B4), one has

$$\int_{\epsilon f}^{\infty}\mathrm{d}y\,\hat{\psi} \sim -2(a\sin\epsilon f + b\cos\epsilon f)_{Y=0} + \frac{1}{2\pi}\int_0^{\infty}\mathrm{d}Y\int_0^{2\pi}\mathrm{d}\psi^{(0)}\frac{1}{\psi_y^{(0)}}H^{(0)}, \tag{B 6}$$

where

$$\begin{aligned} H^{(0)} &= -\frac{\partial}{\partial\psi}\int_{-\infty}^{x}\mathrm{d}x'y'\left(a_T'y_a' + b_T'y_b'\right) - \int_{-\infty}^{x}\mathrm{d}x'\left(a_T'y_a' + b_T'y_b'\right) \\ &\quad + y\frac{\partial}{\partial\psi^{(0)}}\int_{-\infty}^{x}\mathrm{d}x'\left(a_T'y_a' + b_T'y_b'\right). \end{aligned}$$

Also,

$$\mu^2\int_{\epsilon f}^{\infty}\mathrm{d}y\int_{-\infty}^{x}\left.\frac{\hat{\psi}_T}{\psi_y^{(0)}}\right|_{\psi^{(0)}}\mathrm{d}x' \sim \frac{1}{2\pi}\int_0^{\infty}\mathrm{d}Y\int_{-\infty}^{x}\mathrm{d}x'\int_0^{2\pi}\mathrm{d}\psi^{(0)}\frac{1}{\psi_y^{(0)}}\frac{\hat{\psi}_T'}{\psi_y^{(0)\prime}}. \tag{B 7}$$

Combining then (B5) with (B6) and (B7), and making further use of (B4), yields (5.5*c*).

REFERENCES

BAINES, P. G. 1987 Upstream blocking and airflow over mountains. *Ann. Rev. Fluid Mech.* **19**, 75.

BAINES, P. G. & HOINKA, K. P. 1985 Stratified flow over two-dimensional topography in fluid of infinite depth: a laboratory simulation. *J. Atmos. Sci.* **42**, 1614.

CLARK, T. L. & PELTIER, W. R. 1977 On the evolution and stability of finite-amplitude mountain waves. *J. Atmos. Sci.* **34**, 1715.

DRAZIN, P. G. & REID, W. H. 1981 *Hydrodynamic Stability*. Cambridge University Press.

GRIMSHAW, R. H. J. & YI, Z. 1991 Resonant generation of finite-amplitude waves by the flow of a uniformly stratified fluid over topography. *J. Fluid Mech.* **229**, 603.

HOWARD, L. N. & MASLOWE, S. A. 1973 Stability of stratified shear flows. *Boundary-Layer Met.* **4**, 511.

KANTZIOS, Y. D. & AKYLAS, T. R. 1993 An asymptotic theory of nonlinear stratified flow of large depth over topography. *Proc. R. Soc. Lond.* A **440**, 639 (referred to herein as KA).

LAMB, K. G. 1994 Numerical simulations of stratified inviscid flow over a smooth obstacle. *J. Fluid Mech.* **260**, 1.

LAPRISE, R. & PELTIER, W. R. 1989*a* The linear stability of nonlinear mountain waves: Implications for the understanding of severe downslope windstorms. *J. Atmos. Sci.* **46**, 545.

LAPRISE, R. & PELTIER, W. R. 1989*b* The structure and energetics of transient eddies in a numerical simulation of breaking mountain waves. *J. Atmos. Sci.* **46**, 565.

LILLY, D. K. & KLEMP, J. B. 1979 The effects of terrain shape on nonlinear hydrostatic mountain waves. *J. Fluid Mech.* **95**, 241.

LONG, R. R. 1953 Some apects of the flow of stratifed fluids. I. A theoretical investigation. *Tellus* **5**, 42.

MILES, J. W. 1969 Waves and wave drag in stratified flows. In *Proc. 12th Intl Congress of Applied Mechanics*. Springer.

MILES, J. W. & HUPPERT, H. E. 1969 Lee waves in stratified flow. Part 4. Perturbation approximations. *J. Fluid Mech.* **35**, 497.

PIERREHUMBERT, R. T. & BACMEISTER, J. T. 1987 On the realizability of Long's model solutions for nonlinear stratified flow over an obstacle. In *Proc. 3rd Intl Symp. on Stratified Flows* (ed. E. J. List & G. Jirka). ASCE.

PIERREHUMBERT, R. T. & WYMAN, B. 1985 Upstream effects of mesoscale mountains. *J. Atmos. Sci.* **42**, 977.

PRASAD, D. 1996 Dynamics of large-amplitude internal waves in stratified flows over topography. Doctoral dissertation, Department of Mechanical Engineering, MIT.

RAMIREZ, J. 1993 Stability of nonlinear stratified flow over topography. SM thesis, Department of Mechanical Engineering, MIT.

SHAPIRO, R. 1975 Linear filtering. *Math. Comput.* **29**, 1094.

WARN, T. 1983 The evolution of finite amplitude Rossby waves on a weak shear. *Stud. Appl. Maths* **69**, 127.